

Bridging the Homogeneous and Heterogeneous Catalysis by Supramolecular Metal-Organic Cages with Varied Packing Modes

Liang Kan¹, Lei Zhang¹, Long-Zhang Dong¹, Xiao-Han Wang¹, Run-Han Li¹, Chenxing Guo², Xiaopeng Li², Yong Yan^{1}, Shun-Li Li¹, and Ya-Qian Lan^{1*}*

L. Kan, L. Zhang, L.-Z. Dong, X.-H. Wang, R.-H. Li, Y. Yan, S.-L. Li, Y.-Q. Lan

School of Chemistry

South China Normal University

Guangzhou 510006, P. R. China

E-mail: Yong.Yan@m.scnu.edu.cn; E-mail: yqlan@m.scnu.edu.cn

Homepage: <http://www.yqlangroup.com/>

C. Guo, X. Li

College of Chemistry and Environmental Engineering

Shenzhen University

Shenzhen, 518055, P. R. China

Keywords: self-assembly, metal-organic cages, homogeneous catalysis, heterogeneous separation, cycloaddition of CO₂

This article has been accepted for publication and undergone full peer review but has not been through the copyediting, typesetting, pagination and proofreading process, which may lead to differences between this version and the [Version of Record](#). Please cite this article as [doi: 10.1002/adma.202310061](https://doi.org/10.1002/adma.202310061).

This article is protected by copyright. All rights reserved.

Abstract

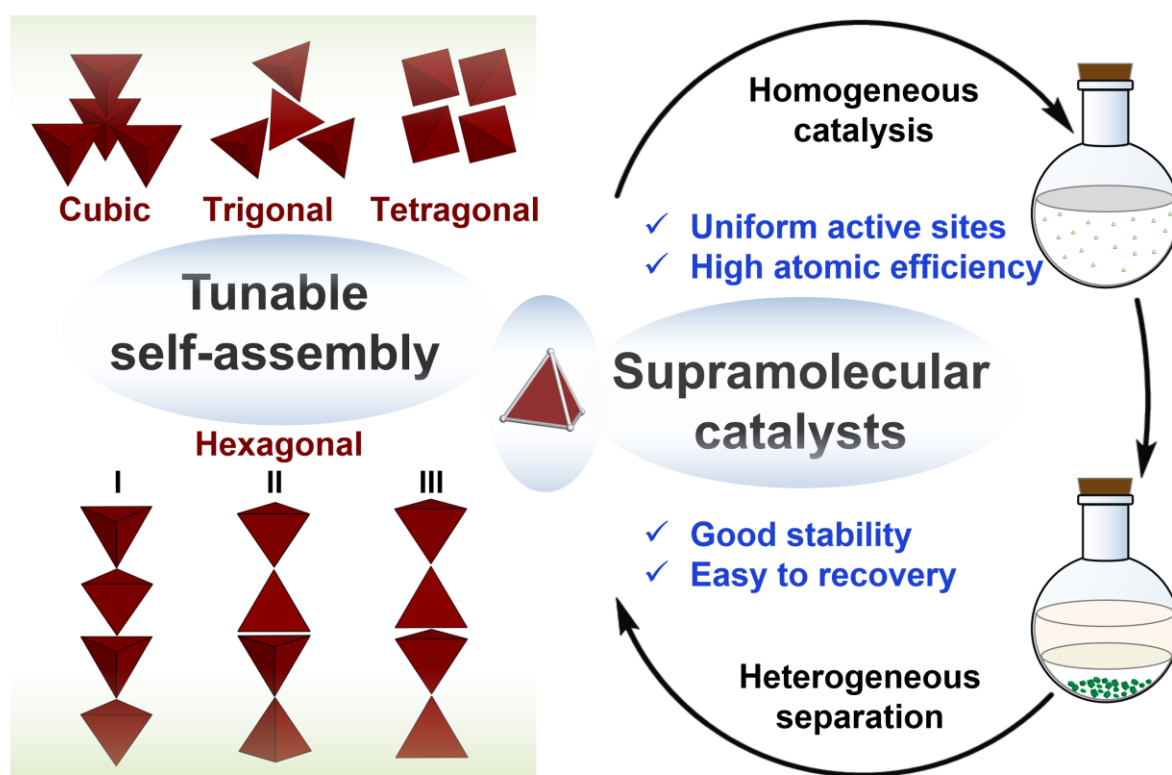
Integrating the advantages of homogeneous and heterogeneous catalysis has proved to be an optimal strategy for developing catalytic systems with high efficiency, selectivity, and recoverability. Supramolecular metal-organic cages (MOCs), assembled by the coordination of metal ions with organic linkers into discrete molecules, have performed solvent processability due to their tunable packing modes, endowing them with the potential to act as homogeneous or heterogeneous catalysts in different solvent systems. Here, we report the design and synthesis of a series of stable $\{\text{Cu}_3\}$ cluster based tetrahedral MOCs with varied packing structures. These MOCs, as homogeneous catalysts, not only show high catalytic activity and selectivity regardless of substrates size during the CO_2 cycloaddition reaction, but also can be easily recovered from the reaction media through separating products and co-catalysts by one-step work-up. This is because that these MOCs have varied solubilities in different solvents due to the tunable packing of MOCs in the solid state. Moreover, the entire catalytic reaction system is very clean, and the purity of cyclic carbonates is as high as 97% without further purification. This work provides a unique strategy for developing novel supramolecular catalysts that can be used for homogeneous catalysis and recycled in a heterogeneous manner.

1. Introduction

Excessive emission of CO_2 is one of the main culprits causing global warming and ocean acidification.^[1] Due to the abundant, non-toxic, and inexpensive characteristics of CO_2 as C_1 feedstock, the chemical conversion of CO_2 is considered to be a prospective approach for reducing CO_2 emission by converting it to form value-added chemicals.^[2] However, the CO_2 conversion is often costly due to its inherent thermodynamic stability.^[3] The chemical fixation of CO_2 with epoxides not only overcomes the thermodynamic drawbacks of CO_2 activation, but also yields high-value products with 100% atomic economy. The products are usually stable cyclic carbonates, which are widely used in pharmaceutical and fine chemical industries as organic synthetic intermediates.^[4] In the past two decades, a large number of catalysts have been developed for the fixation of CO_2 with epoxides, mainly including homogeneous catalysts such as metal salen complexes^[5] and heterogeneous ones such as zeolites, porous organic polymers (POPs),^[6] covalent-organic frameworks (COFs),^[7] and metal-organic frameworks (MOFs).^[8]

Homogeneous catalysts such as well-known metal salen molecules can have an atomic efficiency of nearly 100% and can be designed and optimized more easily on the basis of clear mechanism, making them efficient catalysts for chemical fixation of CO_2 with epoxides. However, the difficulty in catalysts separation and poor recyclability are inevitable disadvantages of these materials. By contrast, heterogeneous catalysts have the advantages of recyclability and easy separation from the

mixture of reactants and products, making them more favored in catalysis research and industry. But most of the chemical conversion in heterogeneous catalysis occurs on the surface of the catalysts, resulting in relatively low atomic utilization and catalytic efficiency. In addition, heterogeneous catalysts often have complex structures causing different behaviors of atoms on the surface and inside the catalyst. Therefore, it is difficult to accurately design the catalytic sites and regulate their surrounding chemical environment, which greatly increases the difficulty in improving the selectivity of products and clarifying the catalytic mechanism. Given the above factors, researchers have been committed to developing new catalysts with high activity, selectivity and reusability.^[9] Although the recent development of heterogeneous single-metal-site catalysts (HSMSCs) provides opportunities to build a bridge between homogeneous and heterogeneous catalysis by fixing single metal sites on heterogeneous supports, their excellent catalytic activity is often achieved at high temperatures. Therefore, in order to perfectly integrate the advantages of homogeneous and heterogeneous catalysts, synthesis of homogeneous catalysts that can be recovered from the system after reaction in a heterogeneous way remains a critical challenge for catalysts discovery.



Scheme 1. Self-assembly of supramolecular tetrahedral metal-organic cages with various packing modes and the system of homogeneous supramolecular MOCs based catalysis coupled with

heterogeneous separation. There are three modes (I, II and III) for the hexagonal packing of tetrahedral cages as observed in the MOCs synthesized in this work and they are different in the orientations of adjacent cages aligned along the unit cell *c* axis.

Supramolecular metal-organic cages (MOCs) composed of metal nodes with various coordination geometries and ligands with distinct size and shape have attracted considerable attention in the field of supramolecular chemistry, showing applications including catalysis, molecular recognition, gas storage and separation, and biomedical applications.^[10] As for catalysis, MOCs with internal cavities and isolated active-sites play the role of nano-sized molecular containers that are beneficial to substrates adsorption, reaction acceleration, reaction intermediates stabilization, and promotion of the product selectivity.^[11] Supramolecular architecture is assembled by isolated cages through interactions between the adjacent cages such as hydrogen-bonding, dipole-dipole interactions, and aromatic π - π interaction. Moreover, the solid-state structure of MOCs with various packing arrangements can be regulated through the induction of different anions, such as Cl^- , Br^- and I^- .^[12] Therefore, due to difference in packing modes and the nature of interactions between cages, the solubility of MOCs in solutions varies greatly, which affects whether they are used as homogeneous or heterogeneous catalysts in liquid reaction system. For example, most of the reported MOCs such as $[\{\text{Zn}_4(\mu_4\text{-O})(\text{TBSC})\}_6\{(\text{MnL})_2(\text{DMF})(\text{H}_2\text{O})\}_6]$ are usually soluble in common polar organic solvents (DMF = *N,N*-dimethylformamide, MeOH, EtOH and CH_2Cl_2) and used as homogeneous catalysts.^[13] There are also some rare examples of water-soluble cages, such as PTC-101, PTC-102 and $[\text{Pd}_6\text{-(RuL}_3)_8]^{28+}$.^[14] In addition, a minority of MOCs such as $[\{\text{M}_4(\mu_4\text{-H}_2\text{O})(\text{TBSC})\}_6[\text{HL}]_8]\cdot\text{G}$ are insoluble in common solvents by introducing functional groups ($-\text{H}_2\text{PO}_3$, $-\text{COOH}$ and $-\text{NH}_2$) to enhance the interaction between cages, which can be used for heterogeneous catalysis and readily recovered from the reaction mixtures.^[15] So achieving heterogenization of homogeneous MOCs catalysts is a feasible strategy through rational design of MOC structures, which can act as the homogeneous catalysts during the reaction and be recyclable and reusable in a heterogeneous manner after catalysis (Scheme 1).

Here, we designed and utilized solvothermal reactions of 1,3,5-tris(4'-hydroxy-5'-formylphenyl)benzene (THB) with C_3 -symmetry, 1,2-diaminocyclohexane (1,2-DACH), and copper(II) salts to construct five supramolecular MOCs, denoted **T-Cu₁₂-ClO₄**, **T-Cu₁₂-NO₃**, **T-Cu₁₂-CF₃SO₃**, **S-Cu₁₂**, and **R-Cu₁₂**. These supramolecular MOCs exhibit gradient changes in solubility of DMF, methanol and acetonitrile. Each Cu₁₂-based cage contains abundant unsaturated Lewis acidic sites (LASs) and

exposed amino functional groups that have been proven to favor the capture and activation of CO₂ in the cycloaddition reaction of CO₂ with epoxides.^[8a,16] Consequently, these MOCs act as homogeneous catalysts for the cycloaddition reaction of CO₂ with epoxides due to the weak interaction between cages. Compared with reported porous catalysts, these homogeneous MOCs not only performed excellent catalysis for the cycloaddition reaction of CO₂ with epoxides under mild conditions, but also showed activity which was not noticeably affected by the size of substrates. More importantly, all catalysts can be easily recovered from the reaction system in a heterogeneous manner. Therefore, the integration of advantages between homogeneous and heterogeneous catalysis is achieved using a series of stable MOCs. We not only confirmed the stability of the catalyst during and after catalytic reactions by electrospray ionization-time-of-flight mass spectrum (ESI-TOF-MS), but also obtained the single crystal X-ray structure of the catalyst, which is very rare in reported homogeneous catalysts. Therefore, this work not only synthesizes new types of stable catalysts with both homogeneous and heterogeneous merits, but also provides a platform for building a bridge between homogeneous and heterogeneous catalysis.

2. Results and Discussion

2.1. Self-assembly and Characterization of MOCs

These MOCs were synthesized by solvothermal reactions of the aldehyde and amine precursors with Cu(II) salts in a one-pot fashion. Heating a mixture of THB, (\pm)-*trans*-1,2-DACH, and Cu(ClO₄)₂·6H₂O in DMF and MeOH at 100 °C for 24 h yielded fusiform single crystals of **T-Cu₁₂-ClO₄**. Similarly, **T-Cu₁₂-NO₃** and **T-Cu₁₂-CF₃SO₃** were synthesized by replacing Cu(ClO₄)₂·6H₂O with Cu(NO₃)₂·4H₂O and Cu(CF₃SO₃)₂, respectively. **S-Cu₁₂** was crystallized as green rodlike single crystals from a mixture of THB, (1*S*,2*S*)-(+)-1,2-DACH, and Cu(NO₃)₂·3H₂O in DMF and MeOH at 100 °C for 24 h. Under similar conditions, **R-Cu₁₂** was successfully synthesized, except for replacing (1*S*,2*S*)-(+)-1,2-DACH with (1*R*,2*R*)-(-)-1,2-DACH (**Figure 1**). All products were collected in a highly crystalline form, washed three times with fresh CH₃CN, and characterized by thermogravimetric analysis (TGA), powder X-ray diffraction (PXRD), ESI-TOF-MS, circular dichroism (CD) spectra, and gas adsorption. Most importantly, the accurate structures of the above five MOCs were confirmed by single crystal X-ray diffraction (SCXRD). The detailed crystal data, including structure refinements, selected bond lengths and angles are listed in Tables S3-S10 and the images of single crystals are shown in Figure

S5. The experimental PXRD for all compounds were in good agreement with the theoretical patterns, which proved the phase purity of as-synthesized samples (Figures S13-S16). TGA revealed that, *T*-Cu₁₂-ClO₄, *T*-Cu₁₂-NO₃, *T*-Cu₁₂-CF₃SO₃, *S*-Cu₁₂ and *R*-Cu₁₂ were stable to 380, 330, 380, 330 and 360 °C after which the samples began to decompose, respectively (Figure S17).

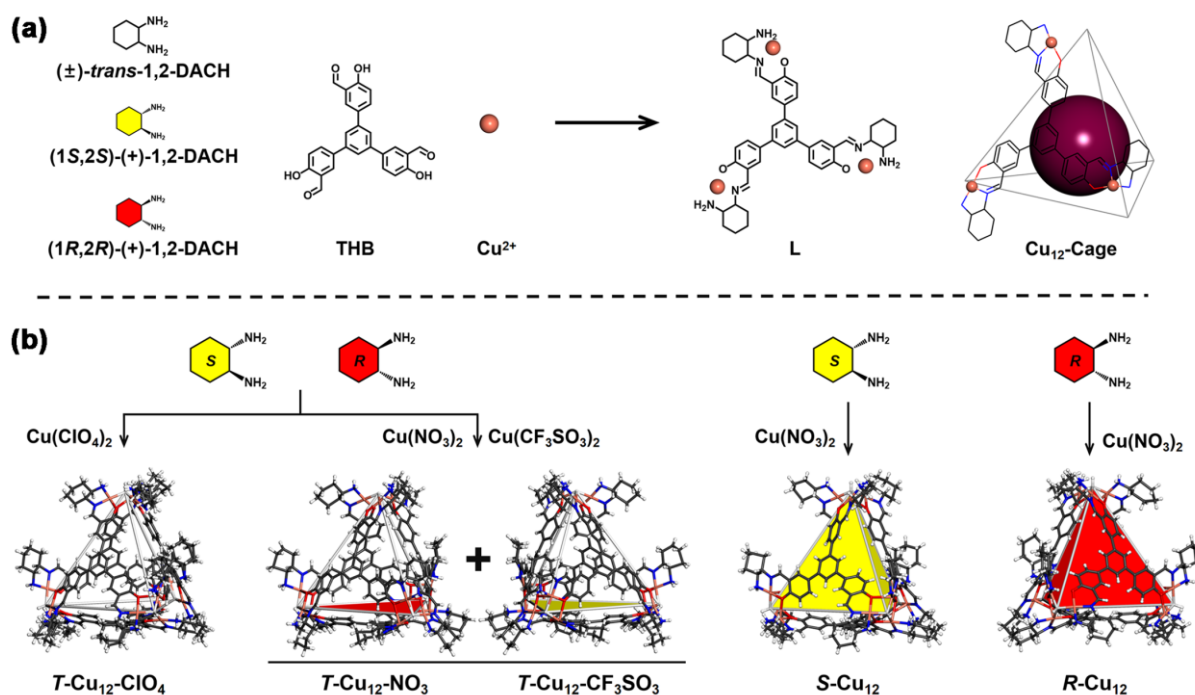


Figure. 1. (a) The self-assembly of the tetrahedral Cu₁₂-based MOCs from 1,2-DACH isomers, THB and Cu²⁺ ions. (b) Self-assembly and single crystal structures of the tetrahedral cages *T*-Cu₁₂-ClO₄, *T*-Cu₁₂-NO₃, *T*-Cu₁₂-CF₃SO₃, *S*-Cu₁₂ and *R*-Cu₁₂.

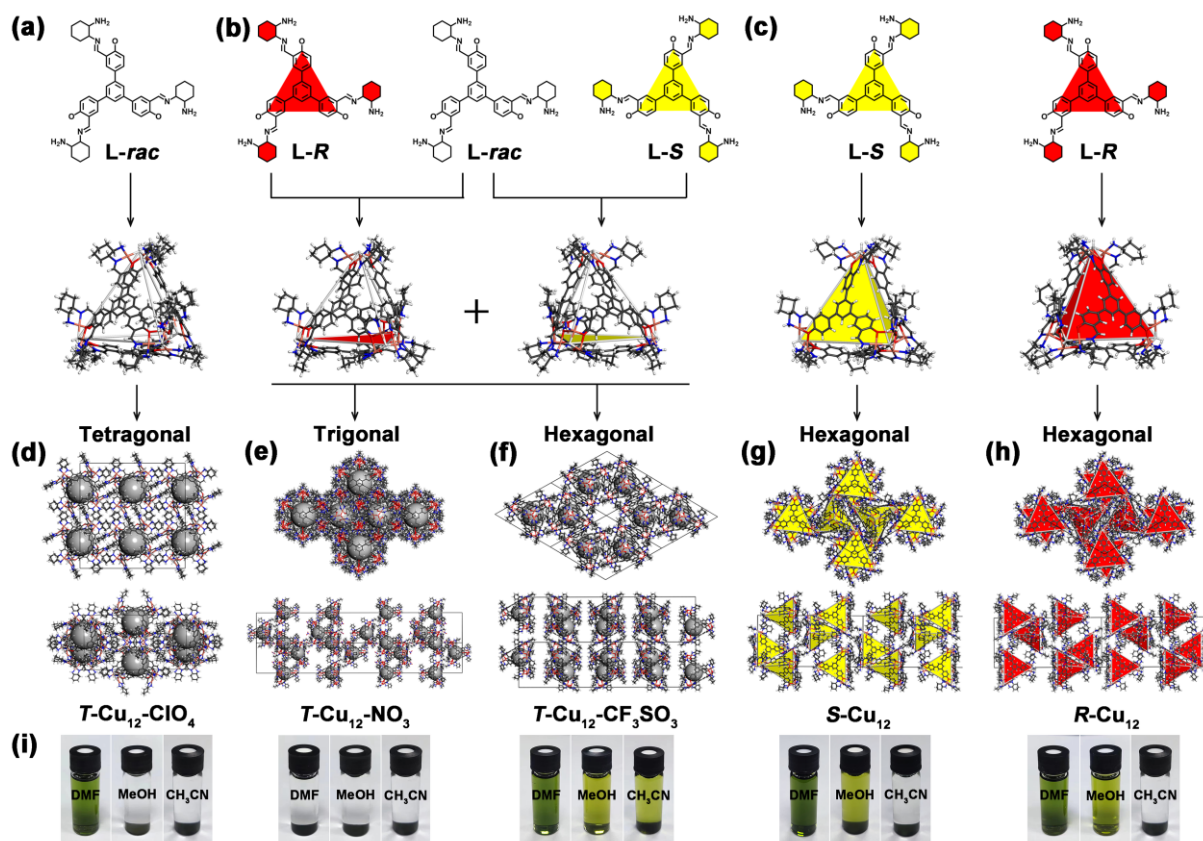


Figure 2. (a-c) The configurations of various ligands and isolated cages in single crystal structures formed during self-assembly. (d-h) The packing modes in single crystal structures of **T-Cu₁₂-ClO₄**, **T-Cu₁₂-NO₃**, **T-Cu₁₂-CF₃SO₃**, **S-Cu₁₂** and **R-Cu₁₂**. (i) Solubility tests for **T-Cu₁₂-ClO₄**, **T-Cu₁₂-NO₃**, **T-Cu₁₂-CF₃SO₃**, **S-Cu₁₂** and **R-Cu₁₂** in DMF, methanol and acetonitrile.

The SCXRD analysis unambiguously indicated that **T-Cu₁₂-ClO₄** with the formation of a tetrahedral cage crystallized in the tetragonal crystal system (space group: $I4_1/a$). Due to the coexistence of (1*S*,2*S*)-(+)-1,2-DACH and (1*R*,2*R*)-(-)-1,2-DACH, the cage of **T-Cu₁₂-ClO₄** resulted in a mesomeric compound. Structurally, the Cu²⁺ ion shows five-coordinated geometry and is coordinated by two nitrogen atoms from 1,2-DACH, two oxygen atoms from the THB unit, and a μ_3 -O atom, and three adjacent Cu²⁺ ions coordinated with a central oxygen atom form the Cu₃(μ_3 -O) cluster. These clusters display two homochiral configurations, including propeller chirality of Λ and Δ (Figure S6). Further, four Cu₃(μ_3 -O) clusters as the vertices connect four **L-rac** ligands to form a mesomeric tetrahedral cage with inner cavity of 13.3 Å, exclusive of the van der Waals radii of atoms, which is soluble in

DMF but not in other common organic solvents including MeOH, CH₃CN, and CHCl₃ (**Figure 2g**). The ESI-TOF-MS spectra in DMF proved that the peaks with continuous charge states from +2 to +4 correspond to the cage molecules [Cu₁₂L₄(OH)₄]⁸⁺·6(ClO₄[−]), [Cu₁₂L₄(OH)₄]⁸⁺·5(ClO₄[−]) and [Cu₁₂L₄(OH)₄]⁸⁺·4(ClO₄[−]), respectively (Figure S19), demonstrating the excellent stability of **T-Cu₁₂-ClO₄** in solution. Same as **T-Cu₁₂-ClO₄**, **T-Cu₁₂-NO₃** was constructed by self-assembly of THB, cyclohexane diamine, and copper ions. The SCXRD analysis revealed that **T-Cu₁₂-NO₃** features two types of tetrahedral cages as a pair of enantiomers and crystallizes in the trigonal crystal system (space group: *R*-3c) (Figure S7). **T-Cu₁₂-NO₃** has the same coordination mode for Cu(II) ions and similar tetrahedral cage as **T-Cu₁₂-ClO₄**. However, unlike the mesomeric configuration of *L-rac* in **T-Cu₁₂-ClO₄**, the absolute configuration of the self-assembled ligand changes after replacing ClO₄[−] with NO₃[−] in the self-assembly process, including *L-rac*, *L-R* and *L-S* with a ratio of 6:1:1. As shown in **Figure 2b**, there are two types of tetrahedral cages in the compound. One cage consists of four Cu₃(μ₃-O) clusters, three *L-rac* ligands, and one *L-R* ligand, while the other one consists of four Cu₃(μ₃-O) clusters, three *L-rac* ligands, and one *L-S* ligand. The configuration of the tetrahedral cages affects the solubility in organic solvents and results in **T-Cu₁₂-NO₃** being insoluble in DMF, which is different from **T-Cu₁₂-ClO₄** (**Figure 2g**). Replacing NO₃[−] with CF₃SO₃[−], another mesomeric MOC (**T-Cu₁₂-CF₃SO₃**) formed. As shown in Figure S8, **T-Cu₁₂-CF₃SO₃** displays the same configuration of ligands and isolated cages as **T-Cu₁₂-NO₃**, but adopts a hexagonal packing mode and is soluble in DMF, MeOH, and CH₃CN. The ESI-TOF-MS spectra in DMF proved that the peaks with continuous charge states from +2 to +4 correspond to the cage molecules [Cu₁₂L₄(OH)₄]⁸⁺·6(CF₃SO₃[−]), [Cu₁₂L₄(OH)₄]⁸⁺·5(CF₃SO₃[−]) and [Cu₁₂L₄(OH)₄]⁸⁺·4(CF₃SO₃[−]), respectively (Figure S20).

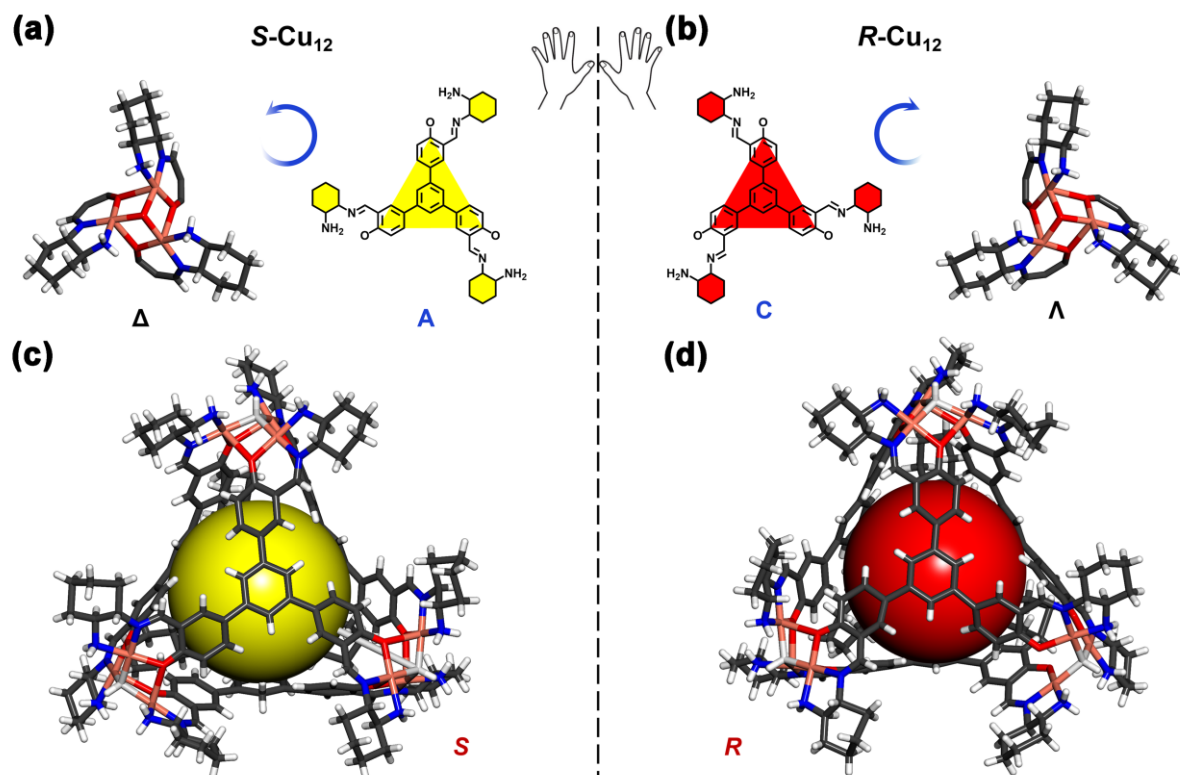


Figure 3. Absolute configurations of propeller chirality (Λ and Δ) and planar chirality (A and C) in the crystal structures of **S-Cu₁₂** (a) and **R-Cu₁₂** (b). Cage structures of **S-Cu₁₂** (c) and **R-Cu₁₂** (d).

Compared to **T-Cu₁₂**, **S-Cu₁₂** and **R-Cu₁₂** were also synthesized by the crystallization of similar tetrahedral cages, and adopted the same coordination pattern of ligands and Cu²⁺ ions (Figure S9 and Figure S10). Unlike the mesomeric **T-Cu₁₂**, **S-Cu₁₂** and **R-Cu₁₂** crystallize in the hexagonal crystal system (space group: $P6_3$) and are homochiral as a pair of enantiomers, which is further demonstrated by circular dichroism (CD) spectra (Figure S21). Both **S-Cu₁₂** and **R-Cu₁₂** are soluble in DMF and MeOH, but not in other organic solvents including CH₃CN, THF, CHCl₃, etc. Due to the enantiotropy of these two structures, only the configuration of **S-Cu₁₂** is described in detail. For **S-Cu₁₂**, three types of chirality of the components are observed, including planar chirality from anticlockwise (A) arrangement of L-S ligands, propeller chirality (Δ) from arrangement of 1,2-DACH around Cu²⁺ ions, and axial chirality from (S)-1,2-DACH (Figure 3a, c). Conversely, clockwise planar chirality (C), propeller chirality (Λ), and (R, R) axial chirality exist in homochiral cage of **R-Cu₁₂** (Figure 3b, d). The ESI-TOF-MS spectra were measured to confirm the formation and stability of cages in

solution. Peaks at m/z of 993.43, 1345.23, and 2048.98 exactly correspond to $[(\text{Cu}_{12}\text{C}_{180}\text{H}_{208}\text{N}_{24}\text{O}_{16})\cdot 4\text{NO}_3]^{4+}$, $[(\text{Cu}_{12}\text{C}_{180}\text{H}_{208}\text{N}_{24}\text{O}_{16})\cdot 5\text{NO}_3]^{3+}$, and $[(\text{Cu}_{12}\text{C}_{180}\text{H}_{208}\text{N}_{24}\text{O}_{16})\cdot 6\text{NO}_3]^{2+}$ ions, respectively, further confirming the stability of these cages in solution (Figure S22 and Figure S23).

2.2. CO₂ Adsorption Capacity of MOCs

The good stability and structural characteristics prompted us to explore their properties as supramolecular catalysts. Previous research has proved that Lewis acid sites (LASs) are beneficial to the adsorption and activation of epoxides through weak coordination with the oxygen atoms from epoxides and Lewis base sites (LBSs) can enhance the interaction with CO₂.^[8a,8d,8e,8h,8i,17] All above MOCs were functionalized with abundant unsaturated metal sites as LASs and amino groups as LBSs, demonstrating their efficient catalytic potential for CO₂ cycloaddition reaction with epoxides. Considering the influence of the binding strength of the catalyst to CO₂ on the cycloaddition reaction, CO₂ adsorption capacity of four MOCs (**T-Cu₁₂-ClO₄**, **T-Cu₁₂-NO₃**, **S-Cu₁₂**, and **R-Cu₁₂**) was investigated at both 273 and 298 K (Figures S24-S27). Corresponding to structural similarity, **S-Cu₁₂** and **R-Cu₁₂** as a pair of enantiomers showed nearly the same adsorption behaviors. CO₂ adsorption capacities for **S-Cu₁₂** and **R-Cu₁₂** were 44.0 cm³/g and 43.2 cm³/g at 273 K, and 30.8 cm³/g and 30.4 cm³/g at 298 K, respectively, while **T-Cu₁₂-ClO₄** and **T-Cu₁₂-NO₃** displayed CO₂ uptakes of 57.4 cm³/g and 51.7 cm³/g at 273 K and 38.2 cm³/g and 31.0 cm³/g at 298 K, respectively. Further, heats (Q_{st}) of CO₂ adsorption were calculated to be 27.2, 31.2, 31.8, and 32.1 kJ/mol for, **T-Cu₁₂-ClO₄**, **T-Cu₁₂-NO₃**, **S-Cu₁₂**, and **R-Cu₁₂**, respectively (Figure S28). Considering the same chemical compositions for the cationic cages in these MOCs, the differences in CO₂ adsorption capacity are related to the difference in the packing modes of the tetrahedral cages. Significantly, the above results for CO₂ adsorption were superior or comparable to many reported porous materials as catalysts for cycloaddition reactions such as Zn-DPA,^[19] Bi-PCN-224^[21] and InDCPN-I,^[20] which implied strong binding affinity between these catalysts and CO₂ and showed the benefit of a porous catalyst compared to a nonporous one.

2.3. Catalytic Performance

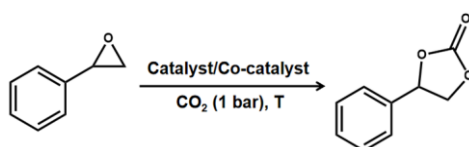
Considering the same $\{\text{Cu}_3\}$ cluster-based vertex structure and chemical composition of the cationic tetrahedral cages for the above MOCs, **R-Cu₁₂** was selected for investigating the catalytic property in the cycloaddition between CO₂ and styrene oxide (SO) as the model substrate under solvent-free conditions. As shown in **Table 1**, a mixture of **R-Cu₁₂** (0.25 mmol%) as the catalyst and tetrabutylammonium bromide (TBAB, 5 mmol%) as the co-catalyst was used for the catalytic cycloaddition reaction under 1 atm of CO₂ atmosphere. The temperature effect on the catalytic activity was explored and only 9% yield was obtained after reaction of 12 h at 40 °C. As the temperature increased from 40 to 80 °C, the catalytic yield of styrene carbonate (SC) could be significantly improved to 97% with a conversion of almost 100% (entries 1-5), indicating 80 °C was the optimum temperature for this catalytic process and was used for the following reactions (Figure S29).

To clarify the effect of the catalyst on catalytic performance, cycloaddition reactions with and without **R-Cu₁₂** were carried out. As shown in entries 6 and 9, the yield of converting SO into SC without adding **R-Cu₁₂** was only 49%, while the catalytic yield increased to 87% dramatically with the addition of only a small amount of catalyst (0.03 mol%), indicating that **R-Cu₁₂** played an important role in accelerating the reaction during the catalytic process (Figure S30). Increase of the amount of the MOC catalyst could improve both the conversion (from 90% to $\geq 99\%$) and yield (from 87% to 97%). Moreover, the reaction time was varied to test the optimal conditions at 80 °C (entries 13-17 and Figure S31). The results displayed that the initial yield of SC was 29% after 2 h. As time increased, the conversion rate eventually reached almost 100% with a selectivity of 97% after 12 h. Furthermore, the control experiments were carried out using only Cu(NO₃)₂ salt and a Cu complex in place of the **R-Cu₁₂** catalyst, respectively (Figure S32 and Figure S33). As shown in entries 7 and 8, the catalytic yields of SC were only 60% and 85%, significantly lower than the yield catalyzed by MOC catalyst (97 %). These results further verified the role of the MOC during the cycloaddition reaction. It is worth noting that the catalyst itself was not soluble in the substrate, but dissolved in the reaction mixture in the presence of TBAB, which resulted in **R-Cu₁₂** being used as a homogeneous catalyst in the cycloaddition reaction. Although many homogeneous catalysts such as metal salen complexes were efficient at catalyzing cycloaddition of CO₂ with epoxides under mild conditions, such catalysts suffered from the difficulty of catalyst separation from the reaction system.^[8,9] In addition, the studies on MOCs as homogeneous catalysts for cycloaddition of CO₂ were rare. In 2021, Cao and co-workers prepared a soluble homogeneous MOC catalyst (ImBDC-Co) for the cycloaddition reaction of CO₂. Although ImBDC-Co functionalized with imidazolium could catalyze

the conversion of SO to SC without the addition of co-catalysts, the yield of SC was only 88% at 120 °C for 24 h due to the saturated coordination of metal sites and low concentration of halogen ions.^[18]

In contrast, **R-Cu₁₂** with abundant unsaturated metal sites as LASs and amino groups as LBSs was conducive to substrate adsorption, CO₂ molecules capture and reaction acceleration, resulting in a high SC yield (97% at 80 °C for 12 h).

Table 1. Cycloaddition reaction of styrene oxide (SO) with CO₂ catalyzed by **R-Cu₁₂**.^a



Entry	Catalyst (mmol%)	TBAB (mmol%)	Temp. (°C)	Time (h)	Conv. (%)	Sel. (%)	Yield (%)
1	0.25	5	40	12	11	82	9
2	0.25	5	50	12	19	89	17
3	0.25	5	60	12	36	94	34
4	0.25	5	70	12	79	96	76
5	0.25	5	80	12	≥99	98	97
6	/	5	80	12	52	94	49
7	Cu(NO ₃) ₂	5	80	12	66	79	60
8	Cu complex ^b	5	80	12	96	89	85
9	0.03	5	80	12	90	97	87
10	0.06	5	80	12	91	98	89
11	0.12	5	80	12	95	98	93
12	0.25	/	80	12			2
13	0.25	5	80	2	31	94	29
14	0.25	5	80	4	59	97	57
15	0.25	5	80	6	78	97	76

16	0.25	5	80	8	90	98	88
17	0.25	5	80	10	95	98	93

^a Reaction conditions: styrene oxide (2 mmol) and CO₂ (1 bar). Conversions, selectivities and yields were determined by ¹H NMR spectra. ^b The Cu complex was synthesized from copper salt, salicylaldehyde and (1*R*,2*R*)-(-)-1,2-diaminocyclohexane by one-step self-assembly (Figure S32).

Surprisingly, unlike traditional homogeneous catalysts, the homogeneous **R-Cu₁₂** cage can be easily recovered from the reaction medium after the completion of reaction. As shown in **Figure 4a**, co-catalysts, catalysts, and catalytic products were separated simultaneously through simple phase transfer operations. A chloroform solution was added to the homogeneous reaction mixture after catalysis, and the catalyst precipitated instantly due to lowered solubility in the above solvents and could be easily separated from the solution. The recovered catalyst was used for the next catalysis cycle and still maintained high catalytic activity of about 97% for the cycloaddition reaction of CO₂ with SO. The catalyst can be recycled for at least 5 times without losing its activity (**Figure 4d**). Subsequently, with the help of their solubility differences in the aqueous and chloroform phases, the co-catalyst of TBAB and cyclic carbonate products were separated from each other by simple separation work-up. ¹H NMR spectroscopy analysis showed that the purity of SC in organic phase was as high as 97%, albeit containing only a small amount of substrate impurity. However, as important as recyclability, stability is another challenge faced by homogeneous catalysts, especially for soluble MOCs. The homogeneous **R-Cu₁₂** cage was very stable during and after catalysis, which was evidenced by ESI-TOF-MS spectra in DMF (Figure S34). Peaks of cage molecules with continuous charge states from +2 to +4 were observed and consistent with those of the as-synthesized **R-Cu₁₂**. After catalysis, the reaction mixture was dispersed in a chloroform solution and then sealed for several days at room temperature. The MOC after catalysis (denoted **R-Cu₁₂-A**) crystallized from above solution and was characterized by SCXRD, revealing an isomeric structure compared with the initial **R-Cu₁₂** with hexagonal packing mode (Figure S11). **R-Cu₁₂-A** showed the same cage structure with **R-Cu₁₂**, but with cubic packing mode in *F*23 space group. This suggests that it is the varied packing mode of the tetrahedral cage for the cage compound after catalysis that enables efficient separation of the catalyst solid from the reaction media. The stability of homogeneous catalyst was generally characterized by UV-vis spectra, ¹H NMR spectroscopy and mass spectra. A combination of

ESI-TOF-MS spectra and single crystal structure analysis confirmed the integrity of the cage structure of **R-Cu₁₂** during catalysis, revealing high structural and catalytic stability and good recyclability.

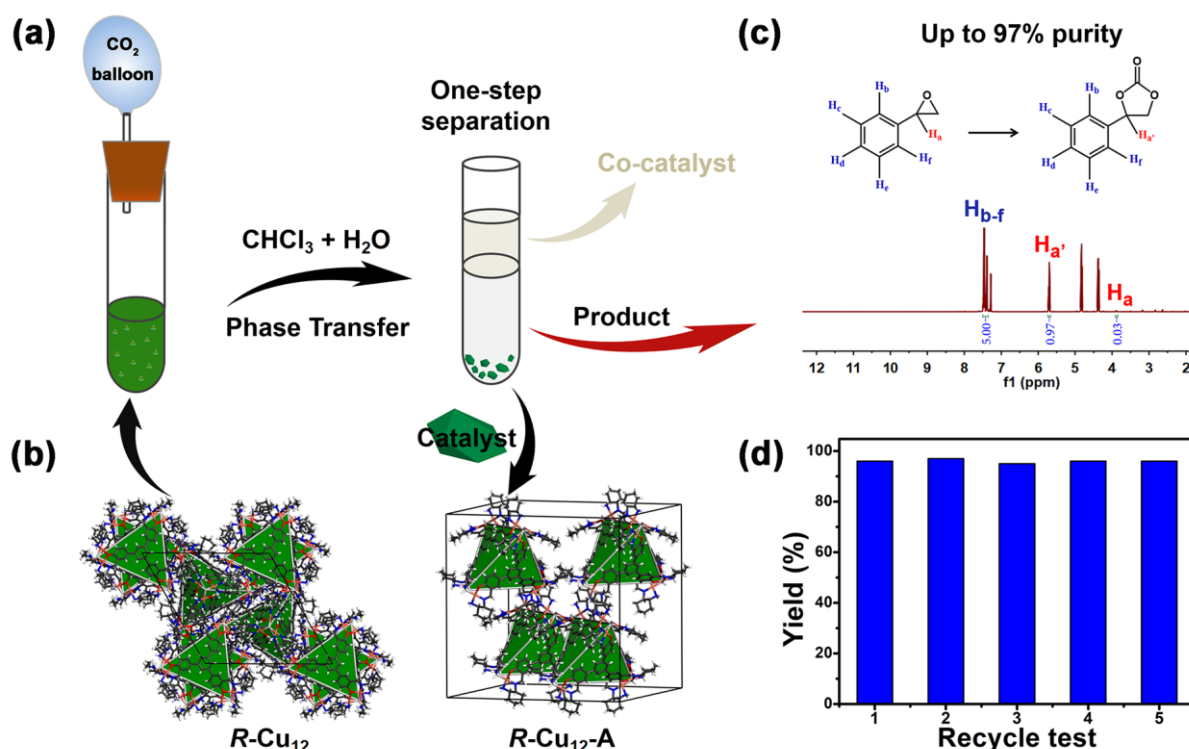


Figure 4. (a) Illustration of achieving one-step separation of catalysts, co-catalysts, and products from initial homogeneous reaction medium. (b) Packing modes of **R-Cu₁₂** and recycled **R-Cu₁₂-A**. (c) ¹H NMR spectra of SC obtained through one-step separation without additional purification. (d) Recycled cycloaddition reaction catalyzed by **R-Cu₁₂**.


Homogeneous catalysts often exhibit better catalytic activity compared with heterogeneous ones. One of the main reasons is that the limited diffusion of substrates into the channels of heterogeneous catalysts makes it difficult for them to contact catalytic sites, which often reduces the catalytic efficiency, especially for the larger substrates.^[8c,8d,8f,16] On the contrary, catalytic activity of homogeneous catalysts is less affected by the size of the substrates. Therefore, in order to investigate the substrate effect on the catalytic activity of cycloaddition reaction for **R-Cu₁₂**, another four terminal epoxides with different sizes (entries 1, 2, 9 and 10 in **Table 2**) were selected to form the corresponding cyclic carbonates. Firstly, control experiments with different temperatures were performed to determine the optimal reaction conditions (Figures S35-S38). As shown in **Table 2**,

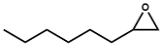
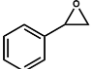
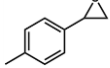
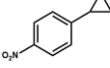
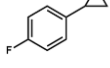
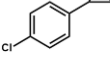
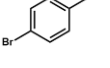
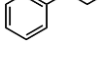
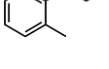
This article is protected by copyright. All rights reserved.

excellent yields of the cyclic carbonates were obtained for both alkyl and aryl epoxides under mild conditions. For the smallest substrate of epichlorohydrin (ECH), the conversion exceeded 99% with 99% yield of the cyclic carbonate. Meanwhile, **R-Cu₁₂** also maintained outstanding catalytic activity for cycloaddition of epoxypropyl phenyl ether (EPE, $9.4 \times 4.3 \text{ \AA}$) and glycidyl 2-methylphenyl ether (GME, $9.8 \times 5.2 \text{ \AA}$) with even larger sizes, showing yields up to 98% and 93% for their corresponding cyclic carbonates, respectively. Subsequently, the control experiments for the cycloaddition reaction of the different epoxides were supplemented (particularly the catalyst loading). As shown in Figures S39-S42, the yield without catalysts was 22% for ECH, 23% for PO, 40% for EPE, and 33% for GME. When a small amount of catalysts (0.06 mmol%) were added, the catalytic yield rapidly increased to 98% for ECH, 80% for PO, 94% for EPE, and 92% for GME. Except for PO, the yield with 0.06 mmol% catalyst almost reached the one with 0.25 mmol% catalyst loading. The above results indicate that **R-Cu₁₂** exhibits good tolerance for substrates and excellent catalytic activity for substrates of different size.

In addition to the size effect of the substrates, molecules with electron donating and withdrawing substituents were also tested for the CO₂ cycloaddition reaction. For 2-(4-methylphenyl)oxirane (4-Me-SO) with electron donating -Me group, the MOC maintained outstanding catalytic activity and afforded 95% yield of the cyclic carbonate (Figure S43). In contrast, electron withdrawing substituents have a noticeable impact on the catalytic activity of the MOC catalysts for cycloaddition reaction. As the electron withdrawing ability of substituents increases ($\text{Br} < \text{Cl} < \text{F} < \text{NO}_2$), the catalytic activity for the corresponding substrate decreases. As shown in entries 5-8 and Figures S44-S47, the yield of corresponding cyclic carbonate was 95% for 4-Br-SO, 93% for 4-Cl-SO, 86% for 4-F-SO, and 81% for 4-NO₂-SO. Without MOC catalysts, the yield of cyclic carbonate was 46% for 4-Me-SO, 28% for 4-Br-SO, 28% for 4-Cl-SO, 23% for 4-F-SO, and 26% for 4-NO₂-SO, emphasizing the role of MOC catalysts during the cycloaddition reaction of CO₂ with a range of epoxides, especially for these epoxides with electron withdrawing substituents.

Table 2. Cycloaddition reaction of various epoxides with CO₂ catalyzed by **R-Cu₁₂**.

Entry	Epoxides (Abbreviation)	Temp. (°C)	Time (h)	Yield (%)
1	 ECH	50	12	>99

2		PO	70	12	>99
3		SO	80	12	97
4		4-Me-SO	80	12	95
5		4-NO ₂ -SO	80	12	81
6		4-F-SO	80	12	86
7		4-Cl-SO	80	12	93
8		4-Br-SO	80	12	95
9		EPE	70	12	98
10		GME	70	12	93

Reaction conditions: catalyst (0.005 mmol), TBAB (0.1 mmol), epoxides (2 mmol) and CO₂ (1 bar). Conversions, selectivities and yields were determined by ¹H NMR spectra.

2.4. Theoretical Calculation

On the grounds of the structural characteristics and excellent catalytic performance, the adsorption sites of CO₂ and SO were investigated during the cycloaddition reaction (**Figure 5a, b**). First, we calculated the binding energy ($\Delta E_{\text{ads}} = -10.1$ kcal/mol) and obtained the corresponding independent gradient model based on Hirshfeld partition (IGMH) analysis, which demonstrated the strong dispersion interactions and hydrogen bonding interactions between CO₂ and the catalyst (-NH₂ and Cu(II) sites). Furthermore, through continuous optimization, we identified four types of the adsorption sites for SO and calculated their corresponding adsorption energy, proving that the

adsorption of SO on -OH and -NH₂ sites was more stable ($\Delta E_{\text{ads}} = -17.2$ kcal/mol). As depicted in **Figure 5b**, the potential energy surface of substrates (SO) during the whole catalytic process was explored by density functional theory (DFT) calculations, and the corresponding catalytic mechanism was proposed. The cycloaddition reaction involved four steps: adsorption, ring-opening, CO₂ insertion and cyclization. Firstly, in the adsorption step, the oxygen atom of SO interacted with the catalyst to form intermediate (int1) with the Gibbs free energy value (ΔG) of -17.2 kcal/mol, and meanwhile the Br⁻ ions of TBAB activated the substrate to generate int2 ($\Delta G = -58.9$ kcal/mol). Next, a ring-opening process occurred through the first transition state (TS-1) to form int3, where the ΔG and the Gibbs activation energy values (ΔG^\ddagger) were 3.6 and 12.3 kcal/mol, respectively. The rate-determining step (RDS) was the CO₂ insertion step, and the energy barrier (ΔG^\ddagger) was 18.8 kcal/mol. The CO₂ molecule attacked the negatively charged oxygen atom of SO in int3, resulting in the formation of intermediate int4 through the transition state TS-2 with ΔG of -20.7 kcal/mol. In the cyclization process, nucleophilic substitution occurred between the nucleophile (the oxygen atom in COO species) and the *beta*-carbon atom ($\beta\text{C}_{(\text{SO})}$, electrophile) of SO to form intermediate int5 through transition state TS-3 (ΔG^\ddagger for int4→TS-3: 12.1 kcal/mol; ΔG for int4→int5: -15.8 kcal/mol) (**Figure 5d**).

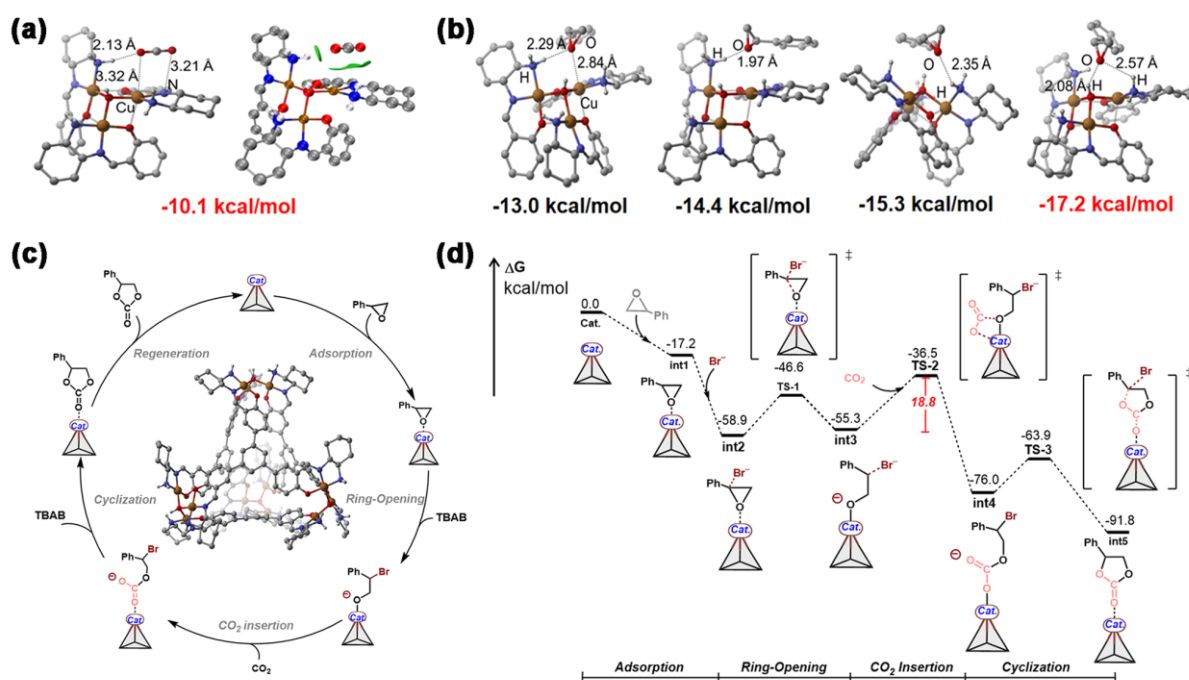


Figure 5. (a) Local views of CO₂ adsorption sites in the tetrahedral cage. (b) Four types of adsorption models for SO. (c) Proposed catalytic mechanism for the cycloaddition of CO₂ with terminal

epoxides. (d) Energy profile diagram of the intermediates and transition states calculated for the cycloaddition of styrene oxide and CO₂.

3. Conclusion

In conclusion, we have designed and constructed five supramolecular MOCs of ***T*-Cu₁₂-ClO₄**, ***T*-Cu₁₂-NO₃**, ***T*-Cu₁₂-CF₃SO₃**, ***S*-Cu₁₂**, and ***R*-Cu₁₂**, which show varied packing modes of {Cu₁₂} based tetrahedral cages in solid state and varied solubility in DMF, methanol and acetonitrile. All these MOCs can serve as homogeneous molecular catalysts for cycloaddition reaction of CO₂ with epoxides, and show excellent catalytic activity and selectivity, recyclability and high structural stability. Computational studies revealed that the vertices structure of the tetrahedral cage formed by trinuclear {Cu₃} cluster facilitates the adsorption of CO₂ and subsequent catalytic processes from adsorption to cyclization. Unlike traditional homogeneous catalysts, these molecular catalysts can be easily recovered from the reaction media by one-step separation of products and co-catalysts. This is because that a poor solvent can induce the formation of a low solubility phase of the MOC with varied packing mode of the tetrahedral cages (ie, from hexagonal to cubic packing mode during the transition from ***R*-Cu₁₂** to ***R*-Cu₁₂-A**). Therefore, this work developed a unique catalytic system that perfectly integrates and advantages of homogeneous and heterogeneous catalysis, and provides a new strategy for designing homogeneous supramolecular MOC catalysts that can be recycled in a heterogeneous manner.

4. Experimental Section

Synthesis of 1,3,5-tris(4'-hydroxy-5'-formylphenyl)benzene (THB): 1,3,5-tris(4'-hydroxy-5'-formylphenyl)benzene (0.85 g, 2.4 mmol) and hexamethylenetetramine (12 g, 85.6 mmol) were dissolved in 80 mL of trifluoroacetic acid (TFA) and the solution was heated at 100 °C for 18 h under N₂. Then 120 mL of HCl (2 M) was added to the above solution and the mixture heated at 100 °C for 3 h under N₂. During this process, beige precipitates appeared. After cooling to room temperature, the beige powder precipitates were collected by filtration, washed with H₂O and EtOH, and finally dried under reduced pressure at 60 °C (0.91 g, 87%). ¹H NMR (600 MHz, [D]DMSO, 25 °C): δ = 10.91 (s, 3H, -OH), 10.34 (s, 3H, -CHO), 8.11 (d, *J* = 6 Hz, 3H, Ar-*H*), 8.06 (dd, *J* = 12, 6 Hz, 3H, Ar-*H*), 7.80 (s, 3H, Ar-*H*), 7.15 (d, *J* = 6 Hz, 3H, Ar-*H*) ppm. ¹³C NMR (150 MHz, [D]DMSO, 25 °C): δ = 192.3, 160.9,

140.9, 135.6, 131.8, 128.1, 123.3, 122.9, 118.3 ppm. HRMS (ESI): calcd. for $C_{27}H_{18}O_6$ ($[M-H]^-$) 437.10, found $[M-H]^-$ 437.10.

*Synthesis of **T-Cu₁₂-ClO₄**, **T-Cu₁₂-NO₃** and **T-Cu₁₂-CF₃SO₃**:* 6.6 mg (0.015 mmol) of THB and 16.7 mg (0.045 mmol) of $Cu(ClO_4)_2 \cdot 6H_2O$ were dissolved in a mixture of DMF (1.3 mL) and methanol (5.7 mL), and then 5.1 mg of (\pm)-trans-1,2-diaminocyclohexane was added to the above mixture. The obtained clear green solution was heated at 100 °C for 24 h. Dark green block crystals of **T-Cu₁₂-ClO₄** were obtained after cooling to room temperature, and washed three times with acetonitrile (63% yield). **T-Cu₁₂-NO₃** and **T-Cu₁₂-CF₃SO₃** were synthesized using the same method for **T-Cu₁₂-ClO₄**, except for replacing ClO_4^- with NO_3^- and $CF_3SO_3^-$, respectively.

*Synthesis of **R-Cu₁₂**:* 6.6 mg (0.015 mmol) of THB and 10.9 mg (0.045 mmol) of $Cu(NO_3)_2 \cdot 3H_2O$ were dissolved in a mixture of DMF (1.1 mL) and methanol (2.4 mL), and then 5.1 mg of (1*R*,2*R*)-(-)-1,2-diaminocyclohexane was added to the above mixture. The obtained clear greensolution was heated at 100 °C for 24 h. Dark green block crystals were obtained after cooling to room temperature, and washed three times with acetonitrile (78% yield).

*Synthesis of **S-Cu₁₂**:* 6.6 mg (0.015 mmol) of THB and 10.9 mg (0.045 mmol) of $Cu(NO_3)_2 \cdot 3H_2O$ were dissolved in a mixture of DMF (1.2 mL) and methanol (2.3 mL), and then 5.1 mg of (1*S*,2*S*)-(+)-1,2-diaminocyclohexane was added to the above mixture. The obtained clear green solution was heated at 100 °C for 24 h. Dark green block crystals were obtained after cooling to room temperature, and washed three times with acetonitrile (75% yield).

*Synthesis of **R-Cu₁₂-A**:* After the cycloaddition reaction using **R-Cu₁₂** as catalyst, dark green block single crystals of **R-Cu₁₂-A** were obtained by adding only $CHCl_3$ to the reaction mixture at room temperature after a few days.

Synthesis of Cu complex: 12 mg (0.05 mmol) of $Cu(NO_3)_2 \cdot 3H_2O$ and 6.1 mg (0.05 mmol) of salicylaldehyde were dissolved in a mixture of ethanol (1 mL) and DMF (0.05 mL), to which 5.7 mg (0.05mmol) of (1*R*,2*R*)-(-)-1,2-diaminocyclohexane was added. The obtained clear solution was heated at 60 °C for 24 h. Blue block crystals were obtained and dried under vacuum (62% yield).

Activation of MOCs for CO₂ absorption: Prior to CO₂ adsorption measurement, about 75 mg of the as-synthesized samples were activated through solvent exchange and degassing processes. The

samples were exchanged with acetonitrile for 3 days. The solvent-exchanged samples were evacuated under high vacuum at 50 °C for 1 h and 100 °C for 12 h to afford the activated samples.

Typical procedure for the cycloaddition reaction of CO₂ with epoxides: The reactions of CO₂ and epoxides were carried out in a Schlenk tube catalyzed by MOCs catalysts in solvent-free environment. In a typical procedure, catalysts (20 mg, 0.005 mmol), TBAB (0.1 mmol) and epoxides (2 mmol) were added to the Schlenk tube (10 mL) equipped with a magnetic stirrer. After the reaction was completed, 15 µL of the reaction mixture was taken to be analyzed in CDCl₃ or [D]DMSO by ¹H NMR. The characteristic peaks of ¹H NMR were analyzed according to literatures.^[16,17,19] For SO and EPE, the conversion, selectivity and yield catalyzed by MOCs catalysts were determined by calculation of the ¹H NMR integrals of the corresponding highlighted protons according to the following equation.

$$\text{Conversion (\%)} = \left(1 - \frac{5I_{H_a}}{I_{H_{b-f}}}\right) \times 100\% \quad (1)$$

$$\text{Selectivity (\%)} = \frac{5I_{H_{a'}}}{I_{H_{b-f}} - 5I_{H_a}} \times 100\% \quad (2)$$

$$\text{Yield (\%)} = \frac{5I_{H_{a'}}}{I_{H_{b-f}}} \times 100\% \quad (3)$$

For GME, 4-Me-SO, 4-F-SO, 4-Cl-SO, 4-Br-SO, 4-NO₂-SO, the yields were determined according to the following equation.

$$\text{Yield (\%)} = \frac{4I_{H_{a'}}}{I_{H_{b-e}}} \times 100\% \quad (4)$$

For ECH and PO, the yield were determined according to the following equation.

$$\text{Yield (\%)} = \frac{I_{H_{a'}}}{I_{H_a} + I_{H_{a'}}} \times 100\% \quad (5)$$

One-step separation (catalysts, co-catalysts, and products) and recycling of catalysts: All the cycloaddition reactions of CO₂ with epoxides catalyzed by MOCs catalysts were homogeneous. After the reaction, additional mixture of CHCl₃ and H₂O was added to the reaction medium and the separation of catalysts, co-catalysts, and products was achieved in one step. Wherein, MOCs catalysts can be precipitated from catalytic system and separated through filtration. The co-catalysts

were left in the aqueous phase, while the products were transferred to the organic phase. After being washed with CHCl_3 and dried, the recycled catalysts were used in the next catalytic reaction.

CCDC contains the supplementary crystallographic data for this paper. These data can be obtained free of charge from The Cambridge Crystallographic Data Centre via www.ccdc.cam.ac.uk/data_request/cif.

Supporting Information

Supporting Information is available from the Wiley Online Library or from the author.

Acknowledgements

This work was financially supported by the National Natural Science Foundation of China (No. 22225109, 22071109 and 22271103).

Conflict of Interest

The authors declare no conflict of interest.

References

- [1] a) S. Chu, Y. Cui, N. Liu, *Nat. Mater.* **2016**, *16*, 16-22; b) V. Humphrey, J. Zscheischler, P. Ciais, L. Gudmundsson, S. Sitch, S. I. Seneviratne, *Nature* **2018**, *560*, 628-631.
- [2] a) J. Francis Kurisingal, H. Kim, J. Hyeak Choe, C. Seop Hong, *Coord. Chem. Rev.* **2022**, *473*; b) M. Ding, R. W. Flaig, H. L. Jiang, O. M. Yaghi, *Chem. Soc. Rev.* **2019**, *48*, 2783-2828.
- [3] a) N. von der Assen, J. Jung, A. Bardow, *Energy Environ. Sci.* **2013**, *6*.
- [4] a) R. R. Shaikh, S. Pornpraprom, V. D'Elia, *ACS Catalysis* **2017**, *8*, 419-450.

This article is protected by copyright. All rights reserved.

- [5] a) J. A. Castro-Osma, K. J. Lamb, M. North, *ACS Catal.* **2016**, *6*, 5012-5025; b) F. Zhou, S.-L. Xie, X.-T. Gao, R. Zhang, C.-H. Wang, G.-Q. Yin, J. Zhou, *Green Chem.* **2017**, *19*, 3908-3915; c) X. Wu, M. North, *ChemSusChem* **2017**, *10*, 74-78; d) M. North, S. C. Z. Quek, N. E. Pridmore, A. C. Whitwood, X. Wu, *ACS Catal.* **2015**, *5*, 3398-3402.
- [6] G. Ji, Z. Yang, H. Zhang, Y. Zhao, B. Yu, Z. Ma, Z. Liu, *Angew. Chem. Int. Ed.* **2016**, *55*, 9685-9689.
- [7] a) Y.-R. Du, G.-R. Ding, Y.-F. Wang, B.-H. Xu, S.-J. Zhang, *Green Chem.* **2021**, *23*, 2411-2419; b) H. Li, X. Feng, P. Shao, J. Chen, C. Li, S. Jayakumar, Q. Yang, *J. Mater. Chem. A* **2019**, *7*, 5482-5492; c) W. Zhou, Q. W. Deng, G. Q. Ren, L. Sun, L. Yang, Y. M. Li, D. Zhai, Y. H. Zhou, W. Q. Deng, *Nat. Commun.* **2020**, *11*, 4481.
- [8] a) H. He, Q. Sun, W. Gao, J. A. Perman, F. Sun, G. Zhu, B. Aguila, K. Forrest, B. Space, S. Ma, *Angew. Chem. Int. Ed.* **2018**, *57*, 4657-4662; b) J. Liang, R. P. Chen, X. Y. Wang, T. T. Liu, X. S. Wang, Y. B. Huang, R. Cao, *Chem. Sci.* **2017**, *8*, 1570-1575; c) L. Liang, C. Liu, F. Jiang, Q. Chen, L. Zhang, H. Xue, H. L. Jiang, J. Qian, D. Yuan, M. Hong, *Nat. Commun.* **2017**, *8*, 1233; d) Z. Qin, H. Li, X. Yang, L. Chen, Y. Li, K. Shen, *Appl. Catal. B Environ.* **2022**, *307*; e) P. Wu, Y. Li, J. J. Zheng, N. Hosono, K. I. Otake, J. Wang, Y. Liu, L. Xia, M. Jiang, S. Sakaki, S. Kitagawa, *Nat. Commun.* **2019**, *10*, 4362; f) Y. Yuan, J. Li, X. Sun, G. Li, Y. Liu, G. Verma, S. Ma, *Chem. Mater.* **2019**, *31*, 1084-1091; g) G. Zhai, Y. Liu, L. Lei, J. Wang, Z. Wang, Z. Zheng, P. Wang, H. Cheng, Y. Dai, B. Huang, *ACS Catal.* **2021**, *11*, 1988-1994; h) T. Zhang, H. Chen, S. Liu, H. Lv, X. Zhang, Q. Li, *ACS Catal.* **2021**, *11*, 14916-14925; i) J. Zhu, P. M. Usov, W. Xu, P. J. Celis-Salazar, S. Lin, M. C. Kessinger, C. Landaverde-Alvarado, M. Cai, A. M. May, C. Slebodnick, D. Zhu, S. D. Senanayake, A. J. Morris, *J. Am. Chem. Soc.* **2018**, *140*, 993-1003.
- [9] a) C. M. Brown, D. J. Lundberg, J. R. Lamb, I. Kevlishvili, D. Kleinschmidt, Y. S. Alfaraj, H. J. Kulik, M. F. Ottaviani, N. J. Oldenhuis, J. A. Johnson, *J. Am. Chem. Soc.* **2022**, *144*, 13276-13284; b) X. Cui, W. Li, P. Ryabchuk, K. Junge, M. Beller, *Nat. Catal.* **2018**, *1*, 385-397.
- [10] a) E. Benchimol, B. T. Nguyen, T. K. Ronson, J. R. Nitschke, *Chem. Soc. Rev.* **2022**, *51*, 5101-5135; b) E. M. El-Sayed, Y. D. Yuan, D. Zhao, D. Yuan, *Acc. Chem. Res.* **2022**, *55*, 1546-1560; c) S. Lee, H. Jeong, D. Nam, M. S. Lah, W. Choe, *Chem. Soc. Rev.* **2021**, *50*, 528-555; d) J. Liu, Z. Wang, P. Cheng, M. J. Zaworotko, Y. Chen, Z. Zhang, *Nat. Rev. Chem.* **2022**, *6*, 339-356; e) M. Pan, K. Wu, J.-H. Zhang, C.-Y. Su, *Coord. Chem. Rev.* **2019**, *378*, 333-349; f) D. Zhang, T. K. Ronson, Y. Q. Zou, J. R. Nitschke, *Nat. Rev. Chem.* **2021**, *5*, 168-182.

- [11] a) H. Lin, Z. Xiao, K. N. Le, T. H. Yan, P. Cai, Y. Yang, G. S. Day, H. F. Drake, H. Xie, R. Bose, C. A. Ryan, C. H. Hendon, H. C. Zhou, *Angew. Chem. Int. Ed.* **2022**, *61*, e202214055; b) C. Liu, K. Liu, C. Wang, H. Liu, H. Wang, H. Su, X. Li, B. Chen, J. Jiang, *Nat. Commun.* **2020**, *11*; c) X. Qi, R. Zhong, M. Chen, C. Sun, S. You, J. Gu, G. Shan, D. Cui, X. Wang, Z. Su, *ACS Catal.* **2021**, *11*, 7241-7248; d) X. Zhang, X. Dong, W. Lu, D. Luo, X.-W. Zhu, X. Li, X.-P. Zhou, D. Li, *J. Am. Chem. Soc.* **2019**, *141*, 11621-11627.
- [12] Q. Bai, Y. M. Guan, T. Wu, Y. Liu, Z. Zhai, Q. Long, Z. Jiang, P. Su, T. Z. Xie, P. Wang, Z. Zhang, *Angew. Chem. Int. Ed.* **2023**.
- [13] C. Tan, J. Jiao, Z. Li, Y. Liu, X. Han, Y. Cui, *Angew. Chem. Int. Ed.* **2018**, *57*, 2085-2090.
- [14] a) Y. P. He, L. B. Yuan, G. H. Chen, Q. P. Lin, F. Wang, L. Zhang, J. Zhang, *J. Am. Chem. Soc.* **2017**, *139*, 16845-16851; b) K. Li, K. Wu, Y. L. Lu, J. Guo, P. Hu, C. Y. Su, *Angew. Chem. Int. Ed.* **2022**, *61*, e202114070.
- [15] W. Gong, D. Chu, H. Jiang, X. Chen, Y. Cui, Y. Liu, *Nat. Commun.* **2019**, *10*, 600.
- [16] B. Parmar, P. Patel, R. S. Pillai, R. I. Kureshy, N.-u. H. Khan, E. Suresh, *J. Mater. Chem. A* **2019**, *7*, 2884-2894.
- [17] J. Gu, X. Sun, X. Liu, Y. Yuan, H. Shan, Y. Liu, *Inorg. Chem. Front.* **2020**, *7*, 4517-4526.
- [18] H. Y. Tong, J. Liang, Q. J. Wu, Y. H. Zou, Y. B. Huang, R. Cao, *Chem. Commun.* **2021**, *57*, 2140-2143.
- [19] a) K. Takaishi, T. Okuyama, S. Kadosaki, M. Uchiyama, T. Ema, *Org. Lett.* **2019**, *21*, 1397-1401; b) L. Martínez-Rodríguez, J. Otalora Garmilla, A. W. Kleij, *ChemSusChem* **2016**, *9*, 749-755; c) Y. Toda, Y. Komiyama, A. Kikuchi, H. Suga, *ACS Catal.* **2016**, *6*, 6906-6910; d) J. A. Castro-Osma, M. North, X. Wu, *Chem. Eur. J.* **2016**, *22*, 2100-2107.

A series of {Cu₁₂} based tetrahedral (*T_d*) metal-organic cages (MOCs) with varied packing modes are self-assembled, which act as highly active homogeneous catalysts for CO₂ cycloaddition with epoxides. The varied packing of *T_d* cages from hexagonal to cubic mode in the MOC enables one-step

heterogeneous separation of the catalyst, co-catalyst and product, which perfectly bridges the homogeneous and heterogeneous catalysis.

L. Kan, L. Zhang, L.-Z. Dong, X.-H. Wang, R.-H. Li, C. Guo, X. Li, Y. Yan*, S.-L. Li, Y.-Q. Lan*

Bridging the Homogeneous and Heterogeneous Catalysis by Supramolecular Metal-Organic Cages with Varied Packing Modes

